J Mater Sci (2009) 44:5214–5224
DOI 10.1007/s10853-009-3536-2

FERROELECTRICS

Energetic analysis of ferroelectric domain patterns by equivalent inclusion method

Y. Y. Liu · J. Y. Li

Received: 23 March 2009 / Accepted: 30 April 2009 / Published online: 22 May 2009

Abstract The formation of domain configuration in ferroelectrics is a consequence of energy minimization, and critically depends on their transformation strain and spontaneous polarization. In this article, we develop an energetic analysis on ferroelectric domain patterns using equivalent inclusion method, treating ferroelectric domain as an ellipsoidal inhomogeneous inclusion in a ferroelectric matrix. The potential energy of the domain is calculated in terms of its orientation and shape, and the energy minimizing configurations have been identified. Both tetragonal and rhombohedral crystals have been analyzed, and the lamellar domain configurations as predicted by the compatibility analysis have been recovered. Additional energy minimizing states have also been revealed, including needle type of domains and charged domains. Different contributions of strain compatibility and polarization compatibility have also been analyzed.

Introduction

Ferroelectrics are materials with switchable transformation strain and spontaneous polarization. Due to symmetry reduction during ferroelectric phase transition, multiple variants with distinct yet crystallographically equivalent transformation strains and spontaneous polarizations often coexist in a ferroelectric, resulting in complicated domain configuration. Such domain configurations not only reveal intrinsic dipolar interactions in ferroelectric lattice, but may also be engineered for technological applications. For example, it is now well known that relaxor ferroelectric crystals with engineered domain configurations often exhibit much enhanced piezoelectric coefficients and electromechanical coupling factors compared to their single-domain state [1–8], and the 90° domain switching in barium titanate crystal can lead to much higher actuation than linear piezoelectric strain [9–12]. Thus a good understanding on the configuration of ferroelectric domains is important from both scientific and technological point of views.

The formation of domain configuration in ferroelectrics is a consequence of energy minimization, and critically depends on their transformation strain $\boldsymbol{\varepsilon}^{(i)}$ and spontaneous polarization $\mathbf{P}^{(i)}$. It was proposed that for the formation of an energy minimizing domain configuration, the transformation strain and spontaneous polarization across domain wall need to be compatible [13], satisfying

$$\boldsymbol{\varepsilon}^{(i)} - \boldsymbol{\varepsilon}^{(j)} = \frac{1}{2}(\mathbf{a} \otimes \mathbf{n} + \mathbf{n} \otimes \mathbf{a}), \quad (\mathbf{P}^{(i)} - \mathbf{P}^{(j)}) \cdot \mathbf{n} = 0,$$

where $\mathbf{n}$ is the normal of the domain wall, and superscripts (i) and (j) are used to refer to variants at both sides of domain wall. Based on the solutions of the compatibility equations, different domain walls have been classified, and various domain patterns have been constructed [13, 14]. Through classical Landau-Ginzburg-Devonshire theory [15–18] or newly developed unconventional theory [19, 20], the domain configurations of ferroelectrics have also be simulated numerically using phase-field method, which confirmed the compatibility of transformation strain and spontaneous

Y. Y. Liu (✉)
Key Laboratory of Low Dimensional Materials and Application Technology of Ministry of Education, Faculty of Materials, Optoelectronics and Physics, Xiangtan University, Hunan 411105, China
e-mail: yunyaliuxtu@yahoo.com.cn

Present Address:
Y. Y. Liu · J. Y. Li
Department of Mechanical Engineering, University of Washington, Seattle, WA 98195-2600, USA
e-mail: jjli@u.washington.edu

polarization across domain wall. These studies are able to recover many of the experimentally observed domain configurations, with an important exception, the charged domain wall, across which the spontaneous polarization is not compatible. Such charged domain walls are commonly observed in ferroelectric crystals [21–24], and their existence is often attributed to the charge screening effect.

While the domain analysis based on the compatibility of transformation strain and spontaneous polarization is able to analyze the morphology of domain configurations, it cannot predict the energy penalty and stability of domain patterns deviating from the energy-minimizing state, such as charged domain walls. Furthermore, it does not separate the effect of strain compatibility from polarization compatibility, which may play quite different roles in different systems, as we will show later. It does not account for the inhomogeneity arising from the crystalline anisotropy either, which inevitably results in additional disturbance field that is also often ignored in the phase-field simulations. As such, we develop an energetic analysis on ferroelectric domain patterns using equivalent inclusion method [25–27] in this article. In particular, we treat ferroelectric domain as an ellipsoidal inhomogeneous inclusion, and analyze its potential energy versus its orientations and shape aspect ratios. Both tetragonal and rhombohedral crystalline systems have been analyzed, and the lamellar domain configuration as predicted by the compatibility analysis have been recovered. Additional energy minimizing states have also been revealed, including needle type of domains and charged domains, and contributions of strain compatibility and polarization compatibility have also been identified. For example, while the 90° domain in tetragonal $BaTiO_3$ crystal is dominated by strain compatibility, both the 71° and 109° domains in rhombohedral $Pb(Mg_{1/3}Nb_{2/3})O_3$-$PbTiO_3$ (PMN-PT) crystal are dominated by polarization compatibility.

Our article is organized as follows. The constitutive equations governing the behavior of ferroelectric crystals are introduced first in "Ferroelectric constitutive equations", followed by the analysis on ferroelectric inclusion and inhomogeneity problems in "Analysis of ferroelectric inclusion". The equivalent inclusion method is then applied to analyze the energetics of ferroelectric domain patterns in tetragonal and rhombohedral crystals in "Energetic analysis of ferroelectric domains", with numerical examples presented for $BaTiO_3$ and PMN-PT crystals. The article then ends with "Concluding remarks" with summary of our key findings.

Ferroelectric constitutive equations

We consider a ferroelectric crystal with transformation strain $\boldsymbol{\varepsilon}^s$ and spontaneous polarization $\mathbf{P}^s$. Furthermore, the ferroelectric can be deformed by an electric field and polarized by a mechanical stress due to the linear piezoelectricity, resulting in the following constitutive equations,

$$\begin{aligned}\boldsymbol{\varepsilon} &= \mathbf{F}^E\boldsymbol{\sigma} + \mathbf{d}^t\mathbf{E} + \boldsymbol{\varepsilon}^s \\ \mathbf{D} &= \mathbf{d}\boldsymbol{\sigma} + \boldsymbol{\kappa}^\sigma\mathbf{E} + \mathbf{P}^s,\end{aligned} \tag{1}$$

where $\boldsymbol{\varepsilon}$ and $\boldsymbol{\sigma}$ are strain and stress, respectively, $\mathbf{D}$ and $\mathbf{E}$ are electric displacement and electric field, respectively, and $\mathbf{F}^E$,$\boldsymbol{\kappa}^\sigma$, and $\mathbf{d}$ are elastic compliance measured at constant electric field, dielectric permittivity measured at constant stress, and piezoelectric coefficient, respectively. The superscript t is used to denote tensor transpose. This set of constitutive equations can be inverted, resulting in a new set of constitutive equations,

$$\begin{aligned}\boldsymbol{\sigma} &= \mathbf{C}^D(\boldsymbol{\varepsilon} - \boldsymbol{\varepsilon}^s) - \mathbf{h}^t(\mathbf{D} - \mathbf{P}^s) \\ \mathbf{E} &= -\mathbf{h}(\boldsymbol{\varepsilon} - \boldsymbol{\varepsilon}^s) + \boldsymbol{\zeta}^\varepsilon(\mathbf{D} - \mathbf{P}^s).\end{aligned} \tag{2}$$

Both sets of the constitutive equations can be rewritten in a concise matrix form,

$$\mathbf{Y} = \mathbf{M}\mathbf{X} + \mathbf{Y}^s,\ \mathbf{X} = \mathbf{L}(\mathbf{Y} - \mathbf{Y}^s), \tag{3}$$

with

$$\mathbf{Y} = \begin{bmatrix}\boldsymbol{\varepsilon} \\ \mathbf{D}\end{bmatrix},\quad \mathbf{X} = \begin{bmatrix}\boldsymbol{\sigma} \\ \mathbf{E}\end{bmatrix},\quad \mathbf{Y}^s = \begin{bmatrix}\boldsymbol{\varepsilon}^s \\ \mathbf{P}^s\end{bmatrix},$$

and

$$\mathbf{M} = \begin{bmatrix}\mathbf{F}^E & \mathbf{d}^t \\ \mathbf{d} & \boldsymbol{\kappa}^\sigma\end{bmatrix},\quad \mathbf{L} = \mathbf{M}^{-1} = \begin{bmatrix}\mathbf{C}^D & -\mathbf{h}^t \\ -\mathbf{h} & \boldsymbol{\zeta}^\varepsilon\end{bmatrix},$$

where the superscript -1 is used to denote matrix inversion. Notice that the constitutive moduli $\mathbf{M}$ and $\mathbf{L}$ are both positive definite, making it convenient to analyze the energetics of ferroelectric domain patterns using these constitutive equations.

Analysis of ferroelectric inclusion

Inclusion, inhomogeneity, and inhomogeneous inclusion

A domain in a ferroelectric is a subregion with distinct transformation strain and spontaneous polarization. To facilitate the analysis, we consider a subregion in a ferroelectric with identical electromechanical moduli $\mathbf{L}$ as the surround matrix, but having different transformation strain $\boldsymbol{\varepsilon}^s$ and spontaneous polarization $\mathbf{P}^s$, as shown in Fig. 1a. We refer such a subregion as an 'inclusion' in the ferroelectric matrix. Without loss of generality, we assume the transformation strain and spontaneous polarization in the matrix are zero. Due to the possible mismatch in the transformation strain and spontaneous polarization between the inclusion and matrix, a disturbance electromechanical field may be

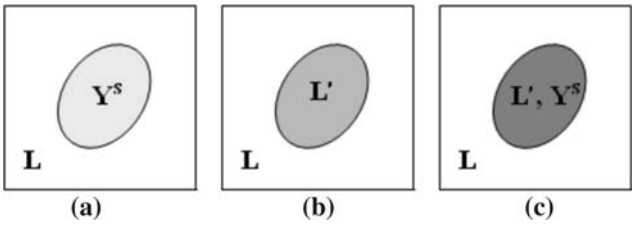

Fig. 1 The schematics of inclusion (**a**), inhomogeneity (**b**), and inhomogeneous inclusion (**c**) in a ferroelectric matrix

induced in both the inclusion and matrix. When the inclusion is ellipsoidal in shape with uniform transformation strain and spontaneous polarization, it is well known that the disturbance electromechanical field $\mathbf{Y}'$, within the inclusion is also uniform [28, 29], given by [30]

$$\mathbf{Y}' = \mathbf{T}\mathbf{Y}^{\mathrm{s}}, \tag{4}$$

with

$$\mathbf{T} = (\mathbf{N}_2\mathbf{S} - \mathbf{N}_3)\mathbf{N},$$

and

$$\mathbf{N}_2 = \begin{bmatrix} \mathbf{I} & \mathbf{0} \\ \mathbf{e}^{\mathrm{t}} & -\boldsymbol{\kappa}^{\varepsilon} \end{bmatrix}, \quad \mathbf{N}_3 = \begin{bmatrix} \mathbf{0} & \mathbf{0} \\ \mathbf{e}^{\mathrm{t}} & -\boldsymbol{\kappa}^{\varepsilon} \end{bmatrix},$$

$$\mathbf{N} = \begin{bmatrix} \mathbf{I} & -\mathbf{d}(\boldsymbol{\kappa}^{\sigma})^{-1} \\ \mathbf{0} & (\boldsymbol{\kappa}^{\sigma})^{-1} \end{bmatrix}.$$

Furthermore, we have

$$\mathbf{e} = (\mathbf{F}^{\mathrm{E}})^{-1}\mathbf{d}, \quad \boldsymbol{\kappa}^{\varepsilon} = \boldsymbol{\kappa}^{\sigma} - \mathbf{d}^{t}(\mathbf{F}^{\mathrm{E}})^{-1}\mathbf{d}.$$

Notice that $\mathbf{S}$ is the piezoelectric Eshelby's tensors that can be evaluated as functions of electromechanical moduli $\mathbf{L}$ of the matrix and aspect ratios and orientations of the ellipsoidal inclusion [29], and $\mathbf{I}$ consists of second- and forth-rank unit tensors. As a result, the disturbance electromechanical field within the inclusion can be determined from the electromechanical moduli $\mathbf{L}$ of the matrix, the transformation strain, and spontaneous polarization $\mathbf{Y}^{\mathrm{s}}$ of the inclusion, and the shape aspect ratios and orientations of the inclusion.

Now we consider a slightly different scenario, wherein the subregion has identical transformation strain and spontaneous polarization as the surrounding matrix, but has different electromechanical moduli $\mathbf{L}'$, as shown in Fig. 1b. We refer to such a subregion as an 'inhomogeneity' in the ferroelectric matrix. Without the loss of generality, the transformation strain and spontaneous polarization in both the inhomogeneity and matrix are assumed to be zero. In a more general situation, the subregion may be different from the surrounding matrix in both electromechanical moduli $\mathbf{L}'$ and transformation strain and spontaneous polarization $\mathbf{Y}^{\mathrm{s}}$, as shown in Fig. 1c. This is referred to as an 'inhomogeneous inclusion'. Now consider a ferroelectric containing an inhomogeneous inclusion and is subjected to a uniform far-field $\mathbf{X}^0$ that would induce a uniform $\mathbf{Y}^0 = \mathbf{M}\mathbf{X}^0$ in the absence of inhomogeneous inclusion. Because of the existence of the inhomogeneous inclusion, additional disturbance field $\mathbf{Y}'$ will be induced, such that the electromechanical field within the inhomogeneous inclusion is given by

$$\mathbf{X}^0 + \mathbf{X}' = \mathbf{L}'(\mathbf{Y}^0 + \mathbf{Y}' - \mathbf{Y}^{\mathrm{s}}).$$

To determine this disturbance field, Eshelby's equivalent inclusion method [29] will be used. In particular, this inhomogeneous inclusion can be replaced by an equivalent inclusion with fictitious transformation strain and spontaneous $\mathbf{Y}^{**}$. In order to ensure the equivalence in electromechanical field, it is necessary that

$$\begin{aligned} \mathbf{L}'(\mathbf{Y}^0 + \mathbf{Y}' - \mathbf{Y}^{\mathrm{s}}) &= \mathbf{L}(\mathbf{Y}^0 + \mathbf{Y}' - \mathbf{Y}^{\mathrm{s}} - \mathbf{Y}^{**}) \\ &= \mathbf{L}(\mathbf{Y}^0 + \mathbf{Y}' - \mathbf{Y}^{*}), \end{aligned} \tag{5}$$

where

$$\mathbf{Y}^{*} = \mathbf{Y}^{\mathbf{s}} + \mathbf{Y}^{**}.$$

In the equivalent inclusion, the disturbance field can be calculated from Eq. 4, which is substituted into the equivalency Eq. 5 to yield

$$\begin{aligned} \mathbf{Y}^{*} = &[(\mathbf{L} - \mathbf{L}')\mathbf{T} - \mathbf{L}]^{-1}(\mathbf{L}' - \mathbf{L})\mathbf{Y}^0 \\ &- [(\mathbf{L} - \mathbf{L}')\mathbf{T} - \mathbf{L}]^{-1}\mathbf{L}'\mathbf{Y}^{\mathrm{s}}. \end{aligned} \tag{6}$$

Notice that the first term is contributed by heterogeneity in the electromechanical moduli, while the second term is contributed by the heterogeneity in transformation strain and spontaneous polarization. If we have an inhomogeneity instead of inhomogeneous inclusion, the second term in the equation then vanishes.

Energetics of inhomogeneous inclusion

With the disturbance electromechanical field within the inhomogeneous inclusion established, we are ready to analyze its energetics. To this end, we consider a ferroelectric D containing an inhomogeneous inclusion Ω with transformation strain and spontaneous polarization $\mathbf{Y}^{\mathrm{s}}$, and subjected to an external field $\mathbf{X}^0$. The internal energy of the ferroelectric can then be derived as

$$\mathcal{F}^{\mathrm{in}} = \int_D \frac{1}{2}(\mathbf{X}^0 + \mathbf{X}') \cdot (\mathbf{Y}^0 + \mathbf{Y}' - \mathbf{Y}^{\mathrm{s}})\mathrm{d}\mathbf{x},$$

which is further simplified as

$$\mathcal{F}^{\mathrm{in}} = \frac{1}{2}\int_D \mathbf{X}^0 \cdot \mathbf{Y}^0 \mathrm{d}\mathbf{x} + \frac{1}{2}\int_\Omega \mathbf{X}^0 \cdot \mathbf{Y}^{**}\mathrm{d}\mathbf{x} - \frac{1}{2}\int_\Omega \mathbf{X}' \cdot \mathbf{Y}^{\mathrm{s}}\mathrm{d}\mathbf{x}, \tag{7}$$

where $\mathbf{Y}^{**}$ is the fictitious transformation strain and spontaneous polarization introduced for equivalency. We have used the fact that

$$\int_D \mathbf{X}^0 \cdot (\mathbf{Y}' - \mathbf{Y}^s)\mathrm{d}\mathbf{x} = \int_D \mathbf{X}^0 \cdot (\mathbf{Y}' - \mathbf{Y}^s - \mathbf{Y}^{**})\mathrm{d}\mathbf{x} + \int_\Omega \mathbf{X}^0 \cdot \mathbf{Y}^{**}\mathrm{d}\mathbf{x} = \int_\Omega \mathbf{X}^0 \cdot \mathbf{Y}^{**}\mathrm{d}\mathbf{x}$$

to derive the equality, where the first term in the equation vanishes because of the generalized Hill's condition for electromechanical solid [31] and the fact that the average of the disturbance field $\mathbf{X}'$ in the ferroelectric vanishes. The potential energy of the inhomogeneous inclusion can then be derived by subtracting external work from the internal energy,

$$\mathcal{F} = \int_D \left[\frac{1}{2}(\mathbf{X}^0 + \mathbf{X}') \cdot (\mathbf{Y}^0 + \mathbf{Y}' - \mathbf{Y}^s) - \mathbf{X}^0 \cdot (\mathbf{Y}^0 + \mathbf{Y}')\right]\mathrm{d}\mathbf{x},$$

which is further simplified as

$$\mathcal{F} = -\frac{1}{2}\int_D \mathbf{X}^0 \cdot \mathbf{Y}^0 \mathrm{d}\mathbf{x} - \frac{1}{2}\int_\Omega \mathbf{X}^0 \cdot \mathbf{Y}^{**}\mathrm{d}\mathbf{x} - \frac{1}{2}\int_\Omega \mathbf{X}' \cdot \mathbf{Y}^s \mathrm{d}\mathbf{x} - \int_\Omega \mathbf{X}^0 \cdot \mathbf{Y}^s \mathrm{d}\mathbf{x}.$$

The energy variation due to the emergence of the inhomogeneous inclusion thus is given by

$$\Delta\mathcal{F} = -\frac{1}{2}\int_\Omega \mathbf{X}^0 \cdot \mathbf{Y}^{**}\mathrm{d}\mathbf{x} - \frac{1}{2}\int_\Omega \mathbf{X}' \cdot \mathbf{Y}^s \mathrm{d}\mathbf{x} - \int_\Omega \mathbf{X}^0 \cdot \mathbf{Y}^s \mathrm{d}\mathbf{x}, \tag{8}$$

which provides a method to evaluate the energetics of ferroelectric domain patterns, as we discuss in detail in the next section.

Energetic analysis of ferroelectric domains

We now apply the equivalent inclusion method to analyze the energetics of domain patterns in ferroelectric crystals, including tetragonal crystal such as $BaTiO_3$ and rhombohedral crystal such as PMN-PT.

Tetragonal crystal

We first consider a tetragonal single crystal such as $BaTiO_3$. There are six ferroelectric variants, and the transformation strain and spontaneous polarization of each variant are given by

$$\begin{aligned}
\boldsymbol{\varepsilon}^{(\pm 1)} &= \begin{bmatrix} \beta & 0 & 0 \\ 0 & \alpha & 0 \\ 0 & 0 & \alpha \end{bmatrix}, \quad \mathbf{P}^{(\pm 1)} = \pm P_t \begin{bmatrix} 1 \\ 0 \\ 0 \end{bmatrix}, \\
\boldsymbol{\varepsilon}^{(\pm 2)} &= \begin{bmatrix} \alpha & 0 & 0 \\ 0 & \beta & 0 \\ 0 & 0 & \alpha \end{bmatrix}, \quad \mathbf{P}^{(\pm 2)} = \pm P_t \begin{bmatrix} 0 \\ 1 \\ 0 \end{bmatrix}, \\
\boldsymbol{\varepsilon}^{(\pm 3)} &= \begin{bmatrix} \alpha & 0 & 0 \\ 0 & \alpha & 0 \\ 0 & 0 & \beta \end{bmatrix}, \quad \mathbf{P}^{(\pm 3)} = \pm P_t \begin{bmatrix} 0 \\ 0 \\ 1 \end{bmatrix},
\end{aligned} \tag{9}$$

with respect to the cubic crystallographic axes, where $x_1^c||[100]$,$x_2^c||[010]$, and $x_3^c||[001]$. The superscript $\pm i$ is used to denote different variants, with the variants $+i$ and $-i$ having identical transformation strain but opposite spontaneous polarization. Both 90° and 180° domains are possible in a tetragonal crystal, which we will discuss in detail next. The globe coordinate system is chosen as $x_1||[100]$,$x_2||[010]$, and $x_3||[001]$, as shown in Fig. 2a.

90° domain

To analyze 90° domains, we consider a tetragonal ferroelectric crystal with transformation strain $\boldsymbol{\varepsilon}^{(3)}$, spontaneous polarization $\mathbf{P}^{(3)}$, and electromechanical moduli $\mathbf{L}^{(3)}$, as shown in Fig. 2. When an external electric field $\mathbf{E}_0$ is applied along $x_1||[100]$ direction, a new domain will nucleate with transformation strain $\boldsymbol{\varepsilon}^{(1)}$, spontaneous polarization $\mathbf{P}^{(1)}$, and electromechanical moduli $\mathbf{L}^{(1)}$. This is referred to as the 90° domain, since the polarization of the new domain forms a 90° angle with the original one, as shown in Fig. 2b. Notice that $\mathbf{L}^{(1)}$ and $\mathbf{L}^{(3)}$ are different in the global coordinate system due to the crystalline anisotropy, and are related by the tensor rotation. As such, the

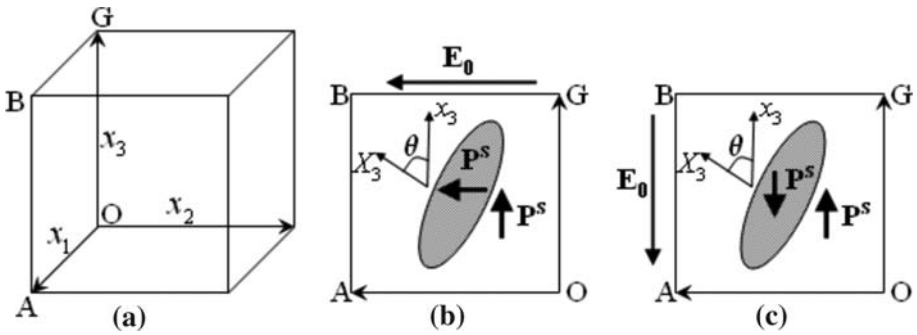

Fig. 2 The schematics of domains in tetragonal ferroelectric crystal (**a**) tetragonal unit cell (**b**) 90°, and (**c**) 180° domains

new domain is regarded as an inhomogeneous inclusion in a ferroelectric matrix, with the effective transformation strain and spontaneous polarization of the inhomogeneous inclusion given by $\boldsymbol{\varepsilon}^{(1)} - \boldsymbol{\varepsilon}^{(3)}$ and $\mathbf{P}^{(1)} - \mathbf{P}^{(3)}$. Under an applied electromechanical loading $\mathbf{X}^0$, the variation of the potential energy due to the emergence of this new domain can be calculated using Eq. (8). We are particularly interested in how the potential energy varies with shape and orientation of the new domain, which provides information on the energy-minimizing domain configuration as well as its stability. To be specific, the new domain is assumed to be spheroidal, and its shape aspect ratio is defined by $a_3/a_1 = a_3/a_2$, with a_i being the dimension along the principal axes of the spheroid. The orientation of the new domain is described by θ, the angle between the x_3 axis of the crystal and X_3, the rotational axis of the spheroid, as shown in Fig. 2b. Noted that both x_2 and X_2 are along [010] direction, and thus we just need one Euler angle to specify the orientation of the new domain.

We carry out the calculation for tetragonal crystal $BaTiO_3$, with its single-domain electromechanical moduli $\mathbf{M}^{(3)}$ and transformation strain and spontaneous polarization listed in Table 1 [32, 33]. The electromechanical moduli $\mathbf{L}^{(1)}$ of the new domain can then be determined from $\mathbf{L}^{(3)}$ using tensor transformation rule. The applied electric field is 6×10^6 V/m, and no stress is applied to the crystal. The variation of potential energy as a function of shape aspect ratio a_3/a_1 and orientation angle θ is shown in Fig. 3. It is observed that there are two wells in the energy landscape when a_3/a_1 approaches zero, one around 45° and the other around −45°. This suggests that lamellar domain is the energy minimizing domain configuration, consistent with many experimental observations. The well at 45° corresponds to an uncharged domain with domain wall along [101], across which the transformation strain and spontaneous polarization are compatible [13], as shown in Fig. 3b. The well at −45°, on the other hand, represents a charged domain with domain wall along $[\bar{1}01]$, which dose not satisfy the compatibility of polarization, as shown in Fig. 3c. Nevertheless, the energy at $\theta = -45°$ (0.21×10^6 J/m^3) is only slightly higher than that at $\theta = 45°$ (-0.22×10^6 J/m^3), and both energy wells are deep and connected by steep energy barrier (5.39×10^6 J/m^3), suggesting that the charged domain is in a metastable state and it is not easy to convert a charged domain to an uncharged one. Indeed such charged domains have often been observed in experiments [21–24].

To further understand such charged domains, we notice that transformation strain is compatible across both uncharged and charged domain walls, and the difference in energy must originate from the spontaneous polarization and the piezoelectricity. To examine this in detail, we present in Fig. 3d the energy variation as function of orientation θ for fully coupled ferroelectric crystal with both spontaneous polarization and piezoelectricity, partially coupled crystal with spontaneous polarization but no piezoelectricity, and the uncoupled ferroelastic crystal with neither spontaneous polarization nor piezoelectricity. As expected, the energy variation of the ferroelastic crystal is symmetric with respect to $\theta = 0°$, and the two wells at −45° and 45° have identical energy regardless of the applied electric field. This is because only the transformation strain exists in the ferroelastic crystal, which is compatible at both orientations. When the spontaneous polarization is included, energy at both well decreases, and the well at 45° (-0.24×10^6 J/m^3) becomes smaller than that at −45° (0.19×10^6 J/m^3), due to additional depolarization energy induced by the incompatibility in polarization across the charged domain wall. If we also take the piezoelectricity into account, which leads to additional piezoelectric strain that may not be compatible across domain walls, the energy changes little near both wells, suggesting that the energy landscape is dominated by the compatibility of transformation strain, and the incompatibility of piezoelectric strain is insignificant. For the fully coupled ferroelectric crystal, we also calculate the energy variation in the absence of any electric field. While the energy well near −45° (4.86×10^6 J/m^3) increases substantially, little change is observed for the energy well near 45° (approaching 0 J/m^3).

Table 1 The electromechanical moduli $\mathbf{M}$ ($\mathbf{F}^E$: 10^{-12} m^2/N; $\mathbf{d}$: 10^{-12} C/N; $\boldsymbol{\kappa}^{\sigma}/\kappa_0$, where $\kappa_0 = 8.85 \times 10^{-12}$ C^2/Nm^2 is the permittivity of free space), transformation strain $\boldsymbol{\varepsilon}$, and spontaneous polarization $\mathbf{P}$ (C/m^2) of tetragonal $BaTiO_3$ single crystal [32, 33]

F^E_{11}	F^E_{12}	F^E_{13}	F^E_{33}	F^E_{44}	F^E_{66}	d_{31}
7.4	−1.4	−4.4	13.1	16.4	7.6	−33.4
d_{33}	d_{15}	$\kappa^{\sigma}_{11}/\kappa_0$	$\kappa^{\sigma}_{33}/\kappa_0$	α	β	P_t
90.0	564.0	4400	129	0.9958	1.0067	0.26

180° domain

Since 90° domain in tetragonal ferroelectric crystal is dominated by the strain compatibility, we also analyze 180° domain in tetragonal crystal, wherein the transformation strain is identical across the domain wall, and only the polarization compatibility is relevant. To this end, we consider an electric field applied along $[00\bar{1}]$ axis, which induces a new domain with electromechanical moduli $\mathbf{L}^{(-3)}$, transformation strain $\boldsymbol{\varepsilon}^{(-3)}$, and spontaneous polarization $\mathbf{P}^{(-3)}$, as shown in Fig. 2c. The variation of potential energy as a function of shape aspect ratio a_3/a_1 and

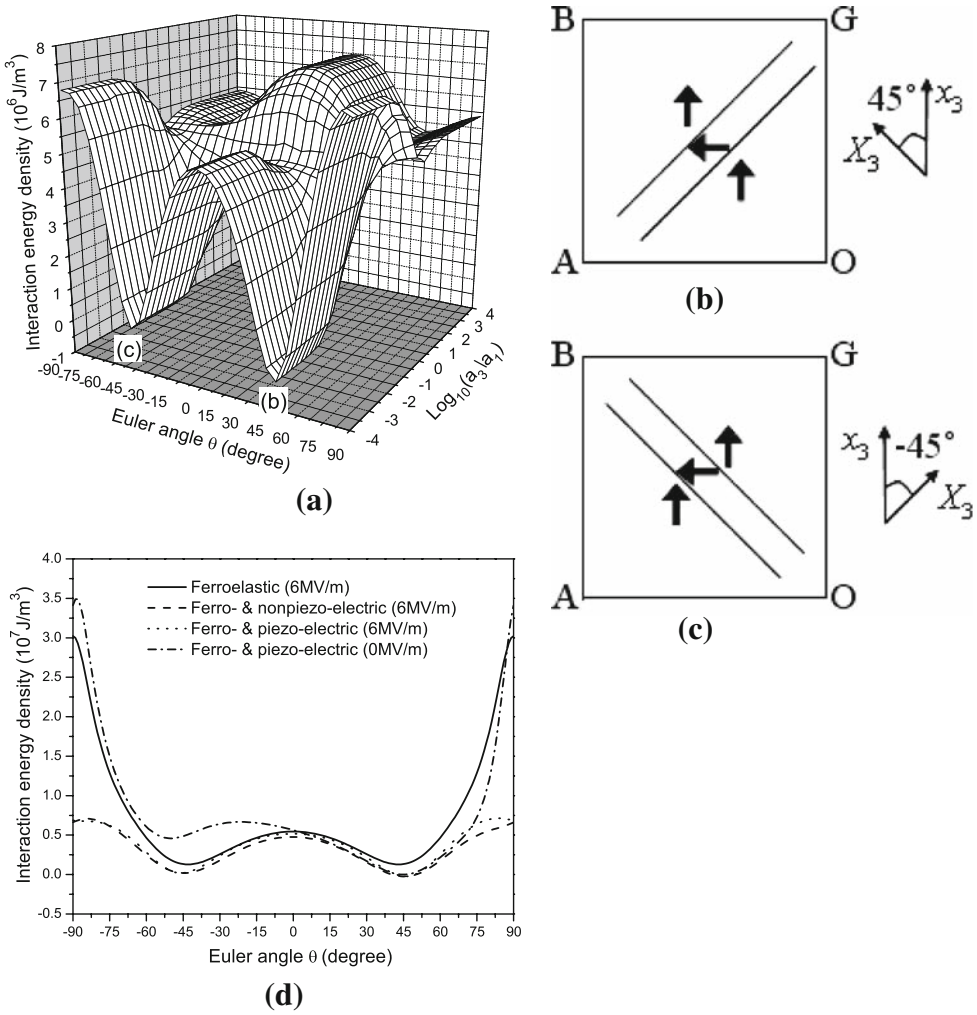

Fig. 3 The potential energy of 90° domain in tetragonal $BaTiO_3$ crystal; **a** the variation of potential energy as a function of shape aspect ratio a_3/a_1 and orientation angle θ; (bc) the schematics of uncharged (**b**) and charged (**c**) domains corresponding to the two wells in the energy landscape; **d** the energy variation with respect to the orientation angle θ of the new domain, at $a_3/a_1 = 10^{-4}$ for ferroelastic, nonpiezoelectric, and ferroelectric crystals

orientation angle θ is shown in Fig. 4. It is observed that there are two wells in the energy landscape. One well resides at $\theta = 90°$ (-2.57×10^6 J/m^3) when a_3/a_1 approaches zero, corresponding to a lamellar domain as shown in Fig. 4b. The other well resides at $\theta = 0°$ (-2.57×10^6 J/m^3) when a_3/a_1 approaches infinity, corresponding to a needle type of domain, as shown in Fig. 4c. To examine both wells in detail, we also plot the variation of potential energy as a function of angle θ at $a_3/a_1 = 10^{-4}$ and $a_3/a_1 = 10^4$, as shown in Fig. 4d. Both wells have similar energy, though the barrier for lamellar domain is much higher. If we ignore the piezoelectricity in the crystal, not much change is observed in the energy variation.

$$
\begin{aligned}
\boldsymbol{\varepsilon}^{(\pm1)} &= \begin{bmatrix} \eta & \delta & \delta \\ \delta & \eta & \delta \\ \delta & \delta & \eta \end{bmatrix}, & \mathbf{P}^{(\pm1)} &= \pm P_r \begin{bmatrix} 1 \\ 1 \\ 1 \end{bmatrix}, \\
\boldsymbol{\varepsilon}^{(\pm2)} &= \begin{bmatrix} \eta & -\delta & -\delta \\ -\delta & \eta & \delta \\ -\delta & \delta & \eta \end{bmatrix}, & \mathbf{P}^{(\pm2)} &= \pm P_r \begin{bmatrix} -1 \\ 1 \\ 1 \end{bmatrix}, \\
\boldsymbol{\varepsilon}^{(\pm3)} &= \begin{bmatrix} \eta & \delta & -\delta \\ \delta & \eta & -\delta \\ -\delta & -\delta & \eta \end{bmatrix}, & \mathbf{P}^{(\pm3)} &= \pm P_r \begin{bmatrix} -1 \\ -1 \\ 1 \end{bmatrix}, \\
\boldsymbol{\varepsilon}^{(\pm4)} &= \begin{bmatrix} \eta & -\delta & \delta \\ -\delta & \eta & -\delta \\ \delta & -\delta & \eta \end{bmatrix}, & \mathbf{P}^{(\pm4)} &= \pm P_r \begin{bmatrix} 1 \\ -1 \\ 1 \end{bmatrix}
\end{aligned}
\tag{10}
$$

Rhombohedral crystal

We then consider rhombohedral ferroelectric crystals such as PMN-PT. There are a total of eight rhombohedral variants, with transformation strain and spontaneous polarization of each variant given by

with respect to the cubic crystallographic axes, where $x_1^c \| [100], x_2^c \| [010]$ and $x_3^c \| [001]$. Three types of domains exist in rhombohedral crystal. The 180° domain is very similar to that of tetragonal crystal, and will not be repeated here. We will focus on 71° and 109° domains in rhombohedral crystal instead. The globe coordinate system is

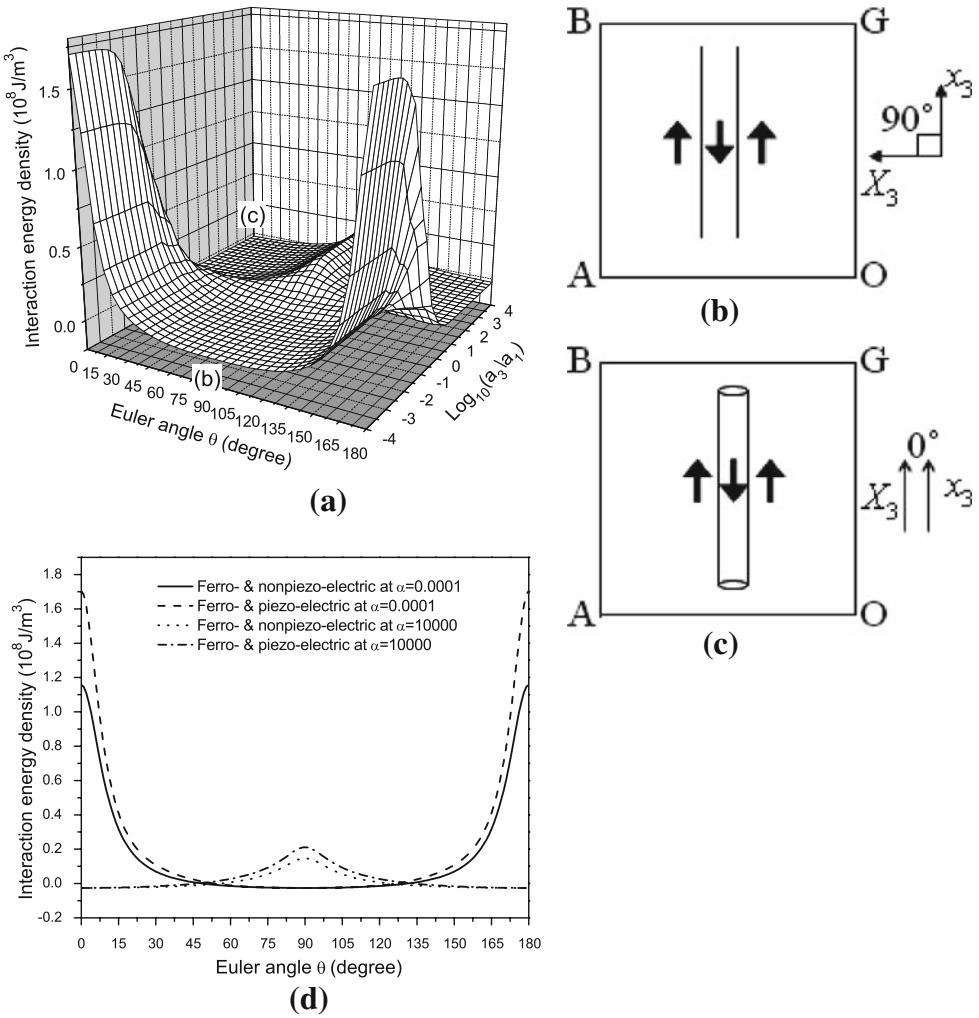

Fig. 4 The potential energy of 180° domain in tetragonal $BaTiO_3$ crystal; **a** the variation of potential energy as a function of shape aspect ratio a_3/a_1 and orientation angle θ; (bc) the schematics of lamellar (**b**) and needle type (**c**) domains corresponding to the two wells in the energy landscape; **d** the energy variation with respect to the orientation angle θ of the new domain, at $a_3/a_1 = 10^{-4}$ and $a_3/a_1 = 10^4$ for nonpiezoelectric and ferroelectric crystals

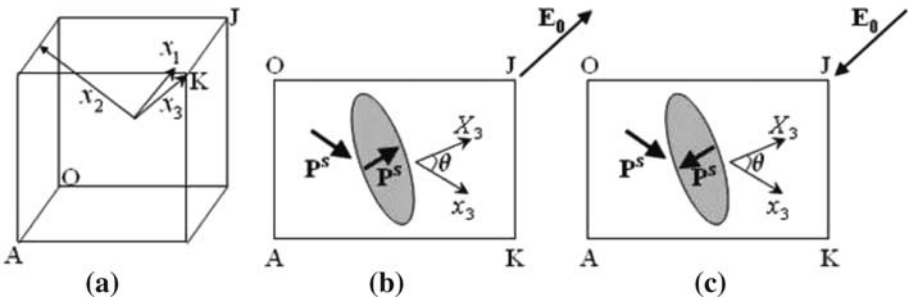

Fig. 5 The schematics of domains in rhombohedral ferroelectric crystal; **a** rhombohedral unit cell, **b** 71° and **c** 109° domains

chosen as $x_1||[\bar{2}11]$,$x_2||[0\bar{1}1]$, and $x_3||[111]$, as shown in Fig. 5a.

71° domain

For 71° domain, we consider a rhombohedral ferroelectric crystal with electromechanical moduli $\mathbf{L}^{(1)}$, transformation strain $\boldsymbol{\varepsilon}^{(1)}$, and spontaneous polarization $\mathbf{P}^{(1)}$, as shown in Fig. 5b. When an external electric field $\mathbf{E}_0$ is applied along the $[\bar{1}11]$, a new 71° domain will nucleate with electromechanical moduli $\mathbf{L}^{(2)}$, transformation strain $\boldsymbol{\varepsilon}^{(2)}$ and spontaneous polarization $\mathbf{P}^{(2)}$, and it can be treated as an inhomogeneous inclusion as we discussed earlier. To be specific, we consider rhombohedral crystal PMN-PT. The single-domain single crystal electromechanical moduli $\mathbf{M}$ of PMN-PT given in coordinate system $x_1^o||[\bar{1}10]$,$x_2^o||[\bar{1}\bar{1}2]$, and $x_3^o||[111]$ are listed in Table 2 [34–39], together with its transformation strain and spontaneous polarization. Notice that the transformation strain [35, 36] is calculated from the lattice parameters of cubic paraelectric phase ($a = 0.401$ nm) [37] and

Table 2 The electromechanical moduli **M** ($\mathbf{F}^E$: 10^{-12} m^2/N; **d**: 10^{-12} C/N; $\boldsymbol{\kappa}^{\sigma}/\kappa_0$, where $\kappa_0 = 8.85 \times 10^{-12}$ C^2/Nm^2 is the permittivity of free space), transformation strain $\boldsymbol{\varepsilon}$, and spontaneous polarization **P** (C/m^2) of rhombohedral PMN-PT single crystal [34–39]

F^E_{11}	F^E_{12}	F^E_{13}	F^E_{14}	F^E_{33}	F^E_{44}	F^E_{66}	d_{31}
62.16	−53.85	−5.58	−166.24	13.34	510.98	232.02	−90
d_{33}	d_{15}	d_{22}	$\kappa^{\sigma}_{11}/\kappa_0$	$\kappa^{\sigma}_{33}/\kappa_0$	η	δ	P_r
190	4100	1340	3950	640	1.00199	0.00079	0.225

rhombohedral ferroelectric phase ($a = 0.402$ nm and $\gamma = 89.91°$) [38].

We first analyze the effects of shape aspect ratio and orientation angle of the 71° domain on its potential energy. The variation of the potential energy as a function of the new domain orientation angle θ and shape aspect ratio a_3/a_1 is given in Fig. 6, and two energy wells are observed. One well resides near $\theta = 35.27°$ (-0.051×10^6 J/m^3) when a_3/a_1 approaches zero, corresponding to a lamellar domain with domain wall along [011] that is energy-minimizing, as shown in Fig 6b. This is consistent with the experimental observations [40]. The other well resides near $\theta = 125.26°$ (0.235×10^6 J/m^3) when a_3/a_1 approaches infinity, corresponding to a needle type domain. A close examination on the energy variation of 71° domain versus the orientation at $a_3/a_1 = 10^{-4}$ and $a_3/a_1 = 10^4$, as shown in Fig. 6d, reveals that the lamellar domain has deep well while the needle domain has shallow well, though the energy level at both wells is similar.

While the lamellar domain is consistent with the analysis based on the compatibility of strain and polarization, the needle type 71° domain is unexpected, since it involves incompatibility in transformation strain across the domain wall. This suggests that for PMN-PT crystal, the strain compatibility is not as important as in $BaTiO_3$, and this is confirmed in Fig. 7. If we only consider a

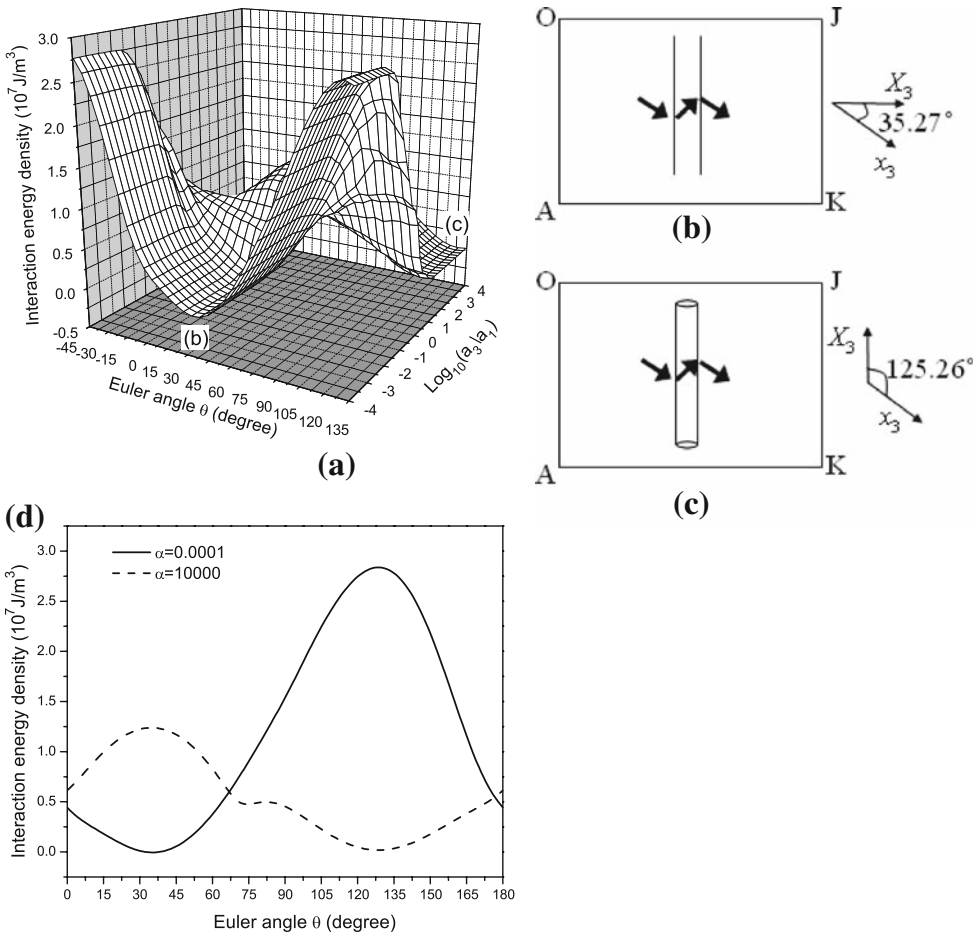

Fig. 6 The potential energy of 71° domain in rhombohedral PMN-PT crystal; **a** the variation of potential energy as a function of shape aspect ratio a_3/a_1 and orientation angle θ; (bc) the schematics of lamellar (**b**) and needle type (**c**) domains corresponding to the two wells in the energy landscape; **d** the energy variation with respect to the orientation angle θ of the new domain, at $a_3/a_1 = 10^{-4}$ and $a_3/a_1 = 10^4$

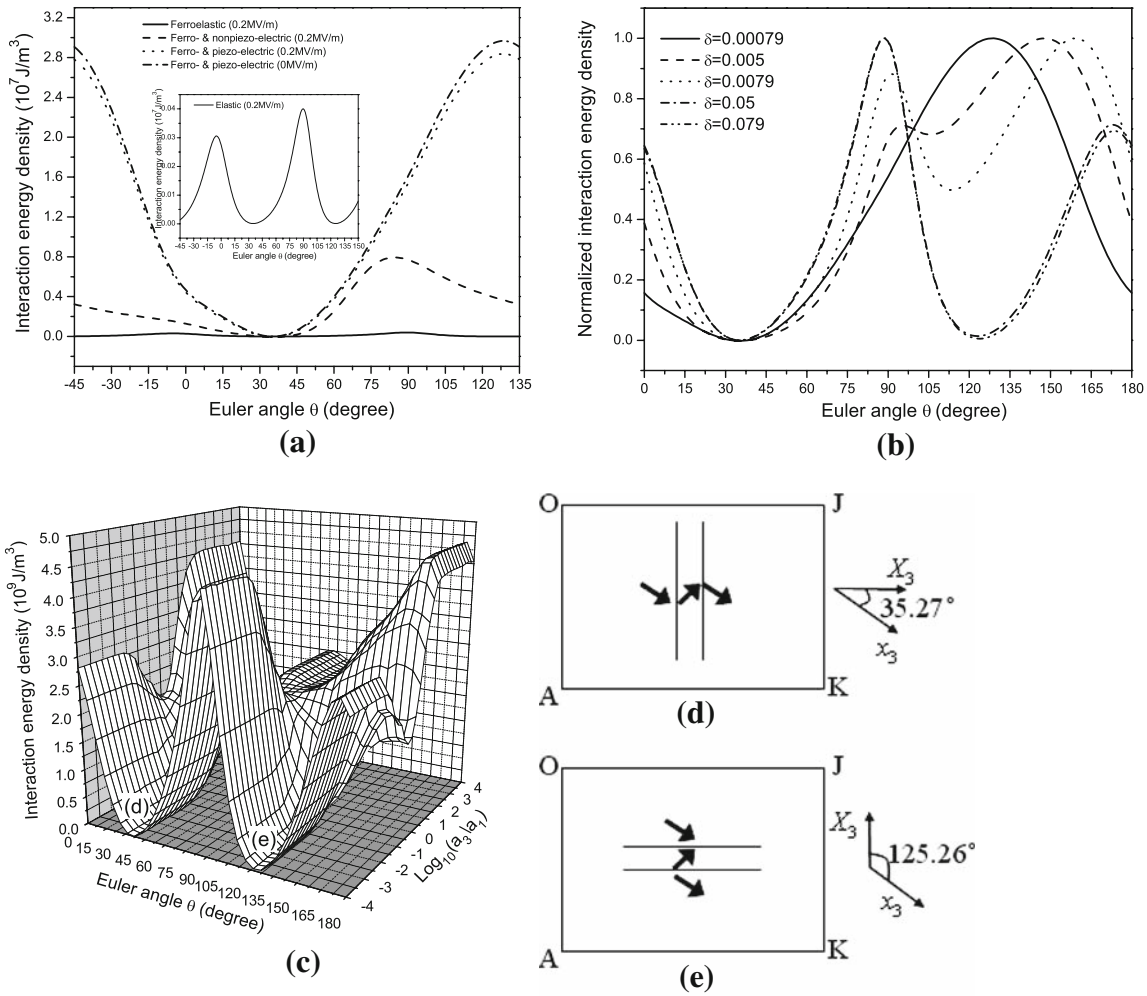

Fig. 7 **a** The energy variation with respect to the orientation θ of the new domain, at $a_3/a_1 = 10^{-4}$ for ferroelastic, nonpiezoelectric, and ferroelectric crystals; **b** the normalized energy variation with respect to the orientation θ of the new domain, at $a_3/a_1 = 10^{-4}$ for different δ values; **c** the variation of potential energy as a function of shape aspect ratio a_3/a_1 and orientation angle θ at $\delta = 0.079$; (de) the schematics of uncharged (**d**) and charged (**e**) 71° domains corresponding to the two wells in the energy landscape in a rhombohedral ferroelectric crystal with $\delta = 0.079$

ferroelastic crystal without coupling with electric field, two energy wells are observed at $\theta = 35.27°$ and $\theta = 125.26°$ when $a_3/a_1 = 10^{-4}$, as shown in the inset of Fig. 7a. However, if we include spontaneous polarization and piezoelectricity in addition to the transformation strain, the energy landscape is substantially changed: one well corresponding to the charged domain disappears, and the other well becomes much deeper, suggesting that 71° domain in PMN-PT crystal is dominated by polarization compatibility, and strain compatibility is insignificant. This is because the value of δ in its transformation strain is rather small. To demonstrate this, we calculate the energy variation for a set of different δ with $a_3/a_1 = 10^{-4}$, and normalize the energy with respect to the maximums of energy at each δ, as shown Fig. 7b. Indeed, with the increased δ, one additional well corresponding to the charged domain gradually appears, and becomes deeper and deeper, indicating increased dominance of strain compatibility. While the well for the uncharged domain resides near $\theta = 35.27°$ and does not shift, the well for the charged domain shift considerably in orientation, and eventually settles near $\theta = 125.26°$ for large δ, as expected from strain compatibility analysis. This suggests that if δ is increased, the needle type domain observed in Fig. 6a may disappears. Indeed this is what we observe in Fig. 7c: the energy well corresponding to the needle domain at a_3/a_1 approaching infinity disappears, and a charged domain corresponding to the well near $\theta = 125.26°$ at a_3/a_1 approaching 0 emerges, as shown in Fig. 7e.

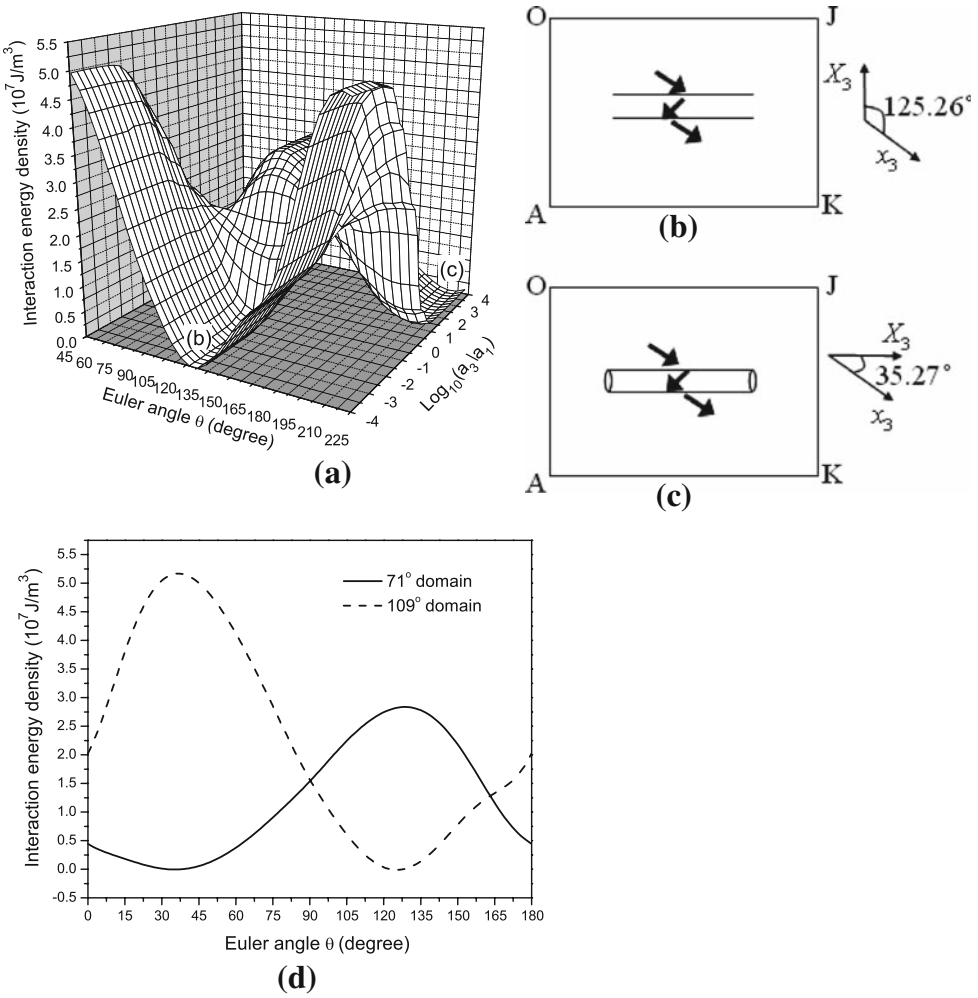

Fig. 8 The potential energy of 109° domain in rhombohedral PMN-PT crystal; **a** the variation of potential as a function of shape aspect ratio a_3/a_1 and orientation angle θ; (bc) the schematics of lamellar (**b**) and needle type (**c**) domains corresponding to the two wells in the energy landscape; **d** the comparison of 71° and 109° domains

109° domain

For 109° domain, we apply an electric field $\mathbf{E}_0$ along $[1\bar{1}\bar{1}]$ instead, and a new 109° domain will nucleate with electromechanical moduli $\mathbf{L}^{(-2)}$, transformation strain $\boldsymbol{\varepsilon}^{(-2)}$ and spontaneous polarization $\mathbf{P}^{(-2)}$, as shown in Fig. 5c. The variation of the potential energy as a function of the new domain orientation angle θ and shape aspect ratio a_3/a_1 is given in Fig. 8, and two energy wells are observed. One well resides near $\theta = 125.26°$ $(-0.1 \times 10^6$ J/m$^3)$ when a_3/a_1 approaches zero, corresponding to a lamellar domain with domain wall along $[00\bar{1}]$ that is energy-minimizing, as shown in Fig. 8b. The other well resides near $\theta = 35.27°$ $(0.09 \times 10^6$ J/m$^3)$ when a_3/a_1 approaches infinity, corresponding to a needle type domain similar to those discussed earlier. The 109° domain is again dominated by polarization compatibility, and the analysis is very similar to 71° domains and will not be repeated here. We also show the comparison between 71° and 109° domains in Fig. 8d, and it is observed the energy at both wells are very close to each other, though 109° domain has much higher energy barrier.

Concluding remarks

In summary, we have developed an equivalent inclusion method to analyze the energetics of ferroelectric domain patterns. We not only identified energy-minimizing lamellar domain configurations as predicted by the compatibility analysis, but also revealed needle type domain configurations and charged domains that are unexpected from the compatibility analysis. The relative effects of strain and polarization compatibilities on the domain patterns have also been analyzed.

Acknowledgement The work is partially supported by NSFC (Approval Nos. 10572124 and 10732100). Liu is also supported by China Scholarship Council Postgraduate Scholarship Program, and Li acknowledges support from NSF (OISE-0820583) and ARO (W911NF-07-1-0410).

References

1. Park SE, Shrout TR (1997) J Appl Phys 82:1804
2. Park SE, Wada S, Cross LE, Shrout TR (1999) J Appl Phys 86:2746
3. Wada S, Park SE, Cross LE, Shrout TR (1999) Ferroelectrics 221:147
4. Wada S, Suzuki S, Noma T, Suzuki T, Osada M, Kakihana M, Park SE, Cross LE, Shrout TR (1999) Jpn J Appl Phys, Part 1 38:5505
5. Liu D, Li JY (2003) Appl Phys Lett 83:1193
6. Liu D, Li JY (2004) Appl Phys Lett 84:3930
7. Liu JJ, Zhou YC, Soh AK, Li JY (2006) Appl Phys Lett 88:032904
8. Wan Q, Chen C, Shen YP (2006) J Mater Sci 41:2993. doi: 10.1007/s10853-006-6766-6
9. Burcsu E, Ravichandran G, Bhattacharya K (2000) Appl Phys Lett 77:1698
10. Ren XB (2004) Nat Mater 3:91
11. Shu YC, Yen JH, Shieh J, Yeh JH (2007) Appl Phys Lett 90:172902
12. Damjanovic D, Budimir M, Davis M, Setter N (2006) J Mater Sci 41:65. doi:10.1007/s10853-005-5925-5
13. Shu YC, Bhattacharya K (2001) Philos Mag B 81:2021
14. Sapriel J (1975) Phys Rev B 12:5128
15. Li YL, Hu SY, Liu ZK, Chen LQ (2001) Appl Phys Lett 78:3878
16. Wang J, Shi SQ, Chen LQ, Li YL, Zhang TY (2004) Acta Mater 52:749
17. Zhang W, Bhattacharya K (2005) Acta Mater 53:185
18. Dayal K, Bhattacharya K (2007) Acta Mater 55:1907
19. Shu YC, Yen JH, Chen HZ, Li JY, Li LJ (2008) Appl Phys Lett 92:052909
20. Yen JH, Shu YC, Shieh J, Yeh JH (2008) J Mech Phys Solids 56:2117
21. Shur VY, Rumyantsev EL, Nikolaeva EV, Shishkin EI (2000) Appl Phys Lett 77:3636
22. Eng LM, Guntherodt HJ (2000) Ferroelectrics 236:35
23. Han JP, Cao WW (2003) Appl Phys Lett 83:2040
24. Iwata M, Katsuraya K, Tachizaki S, Hlinka J, Suzuki I, Maeda M, Yasuda N, Ishibashi Y (2004) Jpn J Appl Phys, Part 1 43:6812
25. Ledbetter H, Dunn ML (1999) Mater Sci Eng A 273–275:222
26. Ledbetter H, Dunn ML (2000) Mater Sci Eng A 285:180
27. Liu YY, Liu JJ, Xie SH, Li JY (2007) Appl Phys Lett 91:172910
28. Wang BA (1992) Int J Solids Struct 29:293
29. Dunn ML, Taya M (1993) Proc R Soc Lond Ser A 443:265
30. Tang LP, Xie SH, Zheng XJ, Zhou YC, Li JY (2008) Mech Mater 40:362
31. Li JY, Dunn ML (1999) Int J Eng Sci 37:665
32. Zgonik M, Bernasconi P, Duelli M, Schlesser R, Gunter P, Garrett MH, Rytz D, Zhu Y, Wu X (1994) Phys Rev B 50:5941
33. Mitsui T, Abe R, Furuhata Y, Gesi K, Ikeda T, Kawabe K, Makita Y, Marutake M, Nakamura E, Nomura S, Sawaguchi E, Shiozaki Y, Tatsuzaki I, Toyoda K (1969) Numerical data and fuctional relationships in sciences and technology. Springer, Berlin
34. Zhang R, Jiang B, Cao WW (2003) Appl Phys Lett 82:787
35. Hane KF, Shield TW (2000) Mater Sci Eng A 291:147
36. Miyazaki S, Kimura S, Otsuka K (1988) Philos Mag A 57:467
37. Han JP, Cao WW (2003) Phys Rev B 68:134102
38. Wasa K, Ito S, Nakamura K, Matsunaga T, Kanno I, Suzuki T, Okino H, Yamamoto T, Seo SH, Noh DY (2006) Appl Phys Lett 88:122903
39. Lu Y, Jeong DY, Cheng ZY, Zhang QM, Luo HS, Yin ZW, Viehland D (2001) Appl Phys Lett 78:3109
40. Shin MC, Chung SJ, Lee SG, Feigelson RS (2004) J Cryst Growth 263:412